# Tutorial: Basic principles, limits of detection, and pitfalls of highly sensitive SQUID magnetometry for nanomagnetism and spintronics

M. Buchner, K. Höfler, B. Henne, et al.

View Online    Export Citation    CrossMark

**ARTICLES YOU MAY BE INTERESTED IN**

CrossMark
click for updates

# Tutorial: Basic principles, limits of detection, and pitfalls of highly sensitive SQUID magnetometry for nanomagnetism and spintronics

M. Buchner, K. Höfler,[a)] B. Henne, V. Ney, and A. Ney[b)]
*Institut für Halbleiter- und Festkörperphysik, Johannes Kepler Universität, Altenberger Str. 69, 4040 Linz, Austria*

In the field of nanomagnetism and spintronics, integral magnetometry is nowadays challenged by samples with low magnetic moments and/or low coercive fields. Commercial superconducting quantum interference device magnetometers are versatile experimental tools to magnetically characterize samples with ultimate sensitivity as well as with a high degree of automation. For realistic experimental conditions, the as-recorded magnetic signal contains several artifacts, especially if small signals are measured on top of a large magnetic background or low magnetic fields are required. In this Tutorial, we will briefly review the basic principles of magnetometry and present a representative discussion of artifacts which can occur in studying samples like soft magnetic materials as well as low moment samples. It turns out that special attention is needed to quantify and correct the residual fields of the superconducting magnet to derive useful information from integral magnetometry while pushing the limits of detection and to avoid erroneous conclusions. © *2018 Author(s). All article content, except where otherwise noted, is licensed under a Creative Commons Attribution (CC BY) license (http://creativecommons.org/licenses/by/4.0/).*
https://doi.org/10.1063/1.5045299

## I. INTRODUCTORY REMARKS

Magnetometry, in general, refers to measuring the magnetization $M$ or the magnetic moment $m$ of a sample. Since both are vectorial quantities, one has to be aware that magnetometry often measures only one component of the magnetization vector. In some cases, e.g., in geology, it is of interest in which direction the magnetization of a piece of rock points. In these cases, a vector magnetometer is the technique of choice and external magnetic fields are less important. However, in many cases, magnetometry is performed in an applied magnetic field and one component, mostly the projection of $M$ onto the field direction, is measured. For the purpose of this Tutorial, magnetometry is distinguished from susceptometry where the magnetic susceptibility $\chi = \partial M / \partial H$ is measured and one can distinguish the (quasi-)static dc-susceptibility, which actually corresponds to magnetometry and the frequency-dependent ac-susceptibility, which is measured in susceptometers.

There are numerous different experimental techniques for magnetometry ranging from vibrating sample magnetometers (VSM),[1] over optical techniques like the magneto-optical Kerr effect (MOKE)[2] to sophisticated experimental techniques utilizing large scale facilities like neutrons (polarized neutron scattering)[3] or synchrotrons (x-ray magnetic circular dichroism).[4] Most of them can be turned into susceptometry by modulating the external magnetic field applied to the specimen and recording the response function $\chi$. This spans from ac-MOKE[5]

to high frequency techniques in the GHz-regime such as electron paramagnetic or ferromagnetic resonance (ESR/FMR).[6,7] For almost any kind of magnetometry, there exists a wealth of textbooks and review articles and here only a subjective choice of exemplarily works has been made; the interested reader is referred to the references therein. It is not the objective of this Tutorial to review and summarize all the types of magnetometry, but to put the focus on one rather common, lab-based magnetometry, namely, the superconducting quantum interference device (SQUID) magnetometer. SQUID magnetometers are commercially available and typically allow a fully automated measurement of the magnetization of a specimen as a function of magnetic field and/or temperature. However, this user-friendly automation comes with the danger of possible pitfalls and artifacts. This Tutorial summarizes some of the most important ones, in particular, if low magnetic fields or small magnetic signals are to be detected. This is predominantly of relevance for those working in the field of nanomagnetism and spintronics, where the detection limit of the SQUID magnetometer is challenged by the physical properties of the typical specimen.

## II. SQUID MAGNETOMETRY

The focus of this Tutorial is to discuss only a limited number of aspects of SQUID magnetometry, in particular, those associated with the superconducting magnet. Therefore, neither the physical principles underlying the use of SQUIDs shall be reviewed nor all potential applications of SQUIDs in different disciplines such as physics, geology, or medicine. The interested reader is referred to a comprehensive review article by Fagley.[8] This article also includes an overview on various technological implementations of SQUIDs for different purposes. For SQUID magnetometry

---
a)Present addresses: Max Planck Institut für Plasmaphysik, Boltzmannstraße 2, 85748 Garching, Germany and Physik-Depatment E28, Technische Universität München, James-Franck-Straße 1, 85748 Garching, Germany.
b)Electronic address: andreas.ney@jku.at. Phone: +43-732-2468-9642. Fax: +43-732-2468-9696.

using a commercial system, a "SQUID system can be considered as a black box that acts like a current (or flux)-to-voltage amplifier with extremely high gain."[8] Over the last few decades, highly sensitive SQUID magnetometers have become essential and widely spread tools to study the magnetic properties of a range of samples including ultrathin films,[9] nanoparticles,[10] and low moment samples like dilute magnetic semiconductors[11] or doped topological insulators.[12] Custom-built superconducting quantum interference device (SQUID) magnetometers, e.g., for ultra-high vacuum chambers,[9] nano-SQUIDs,[13] or ultra-low temperature SQUIDs[11] are sparse. In most cases, in the field of nanomagnetism and spintronics, the standard magnetic characterization relies on SQUID magnetometry utilizing commercially available machines which offer a very good sensitivity together with a high degree of automation.

The most widely used SQUID magnetometer is offered by Quantum Design,[14] the MPMS-XL (approximately 800–1000 sold machines) and more recently, the succeeding model MPMS3 (about 200 sold machines so far). Alternatively, a SQUID magnetometer is also available from Cryogenic,[15] the SX700. No matter which of these machines is used, they commonly utilize a superconducting magnet with no direct measurement of the magnetic field at the location of the sample. Over the recent years, several publications have already been dealing with many possible pitfalls and artifacts of SQUID magnetometers, especially from the MPMS family.[16–23] A known issue of all types of superconducting magnets used in these magnetometers is the remanent or offset field which originates from trapped magnetic flux pinned at defects in the material of the superconducting coil.[23,24] Most importantly, it is directed antiparallel to the last experienced strong field by the magnet. Recording a magnetization curve up to high magnetic fields, this residual field can neither be avoided nor corrected since the commercial SQUID magnetometers do not measure the magnetic field at the location of the sample. The offset field, therefore, leads to an apparent residual hysteresis for diamagnetic samples and an inverted hysteresis for paramagnetic samples[23] which may be held responsible for the possible pitfalls in performing magnetometry using sapphire substrates[20] and limits the ultimate detection sensitivity.[21]

In the following, a detailed characterization of the residual field of the superconducting magnet of an MPMS-XL5 SQUID magnetometer will be presented. On the one hand, it can lead to an erroneous determination of low coercive fields $H_c$. On the other hand, it gives rise to residual signals for low moment samples on diamagnetic substrates. A rather straightforward experiment is presented to quantify the residual field as a function of the history of the magnet. In addition, another possible pitfall in SQUID magnetometry is presented: as pointed out before based on simulations of the expected SQUID response[19,23] that in cases where the magnetization $M$ and the external magnetic field $H$ are not collinear the fitting routine leads to an unrealistic shape of the hysteresis. Finally, once the trapped field has been characterized and the reproducibility of the magnetic measurements has been established, it is demonstrated that it is possible to extract a small magnetic moment even beyond the previously established detection sensitivity for typical low moment

samples.[21] Therefore, the presented experiments are useful for SQUID users which need to rely on the ultimate performance of their SQUID magnetometer to study subtle effects in modern magnetism research.

## A. Measurement principle of SQUID magnetometry

First of all, it is important to note that SQUIDs can only detect magnetic flux $\Phi = \int B \cdot dA$, i.e., magnetic flux density $B$ times the area $A$ of the SQUID loop. Since the effective area $A$ of each SQUID is *per se* not known, it requires that every SQUID magnetometer has to be calibrated with a sample of known magnetic moment and thus known fringing (or stray) field $B$ which is usually done by the manufacturer. Commercial SQUID magnetometers usually detect the *change* of magnetic flux created by mechanically moving the sample through a superconducting pick-up coil which is converted to a voltage $V_{SQUID}$. For the MPMS, the position is denoted as the $x$ direction which is parallel to the external magnetic field $B_{ext}$ so that one obtains raw data, the so-called "lastscan," where $V_{SQUID}$ is plotted versus x-pos. as seen in Fig. 1. To reliably suppress the influence of all kinds of external magnetic fields, the pick-up coil is made as second order gradiometer. The entire detection system is sketched in Fig. 1 and the inset exemplarily shows a single SQUID scan where the maximum of $V_{SQUID}$ at x-pos. of 2 cm corresponds to the sample directly positioned in-between the double coil of the pick-up gradiometer. After mounting a new magnetic specimen, this center position has to be determined using a long scan to properly adjust the sample position with respect to the pickup coils. Note that for the actual measurements, it is in most cases also advisable to record relatively long scans so that not only the maximum but also the two minima are included in the scan. In a day-to-day use, the single SQUID scan is then fitted in a fully automated way without direct access to the routine for the user by assuming that the sample is an ideal point dipole which is exactly positioned on the axis of the magnetometer. The standard software allows one to perform the fit in two ways: it either assumes a fixed sample position and only fits the amplitude of the $V_{SQUID}$(x-pos.)-curve with a single fitting parameter which is
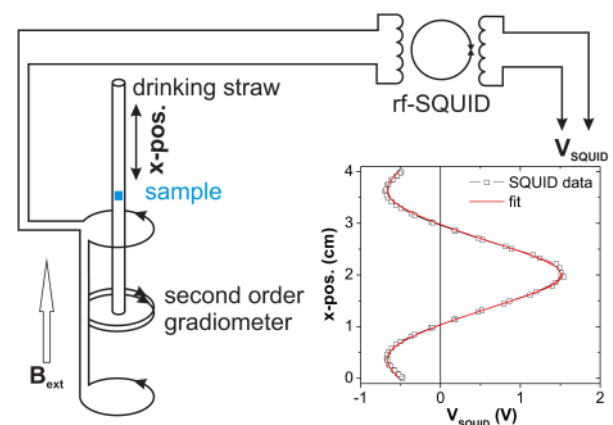


FIG. 1. Schematic setup of a SQUID magnetometer with 2nd order gradiometer. The inset shows the SQUID response $V_{SQUID}$ versus sample position (x-pos.).

the magnetic moment of the assumed point dipole; in the MPMS, this is the so-called linear regression mode. Alternatively, the so-called iterative regression mode also allows the sample position to be fitted together with the amplitude. This has its benefits when temperature dependencies shall be recorded, where the iterative regression mode easily compensates for the thermal expansion of the sample holder assembly. To minimize errors in the fit due to the point dipole approximation in either fitting routine, the specimen size should be limited to max. 5 mm along the scan direction. Laterally, the sample size is naturally limited to 5–6 mm by the sample holder which typically is a clear drinking straw. However, it has been noted from early on that the point dipole approximation leads to incorrect values of the fitted magnetic moment of the sample.[16,18,19] To derive a more accurate value of the magnetic moment of the specimen, correction factors for finite samples sizes have to be used. The details of improved fitting functions, correction factors, and more details about how to derive/calculate them including the relevant formulas can be found in Refs. [16], [18], [19], and [23]. For example, a rather typical cuboid sample size of $5 \times 5 \times 0.5$ mm$^3$ in an in-plane measurement geometry, i.e., applying the magnetic field along one of the 5 mm edges, the correction factor is 0.9833.[23] No matter if the direct result of the automated fitting routine is used or the results are corrected, the fit of each single scan only returns the magnetic moment of the entire sample. To derive the magnetization, which is the more relevant quantity and needed if different samples shall be compared with each other, one has to divide the magnetic moment by the sample volume. However, the sample volume has to be measured independently, which in general is not trivial, especially for a thin film on a (usually) diamagnetic substrate and the associated uncertainty can easily exceed the one stemming from the point dipole approximation.

All measurements in the present work have been taken with the MPMS-XL5 ($\mu_0 H_{max} = 5$ T) magnetometer at the Johannes Kepler University Linz; therefore, all technical remarks only refer to this type of SQUID magnetometer, which is, however, still the most abundant commercial SQUID magnetometer. However, the basic considerations can easily be transferred to other types of magnetometers such as the new MPMS3 or the SX700. For all measurements with the MPMS-XL5, the so-called reciprocal space option (RSO) is used which technically allows one to average over a number of repeated movements of the sample through the pick-up gradiometer within a reasonable time-frame. For highly sensitive measurements, the following parameters turned out to be a good compromise between accuracy and time: 4 cm of sample movement, average over 5 scans with 10 oscillations each at 1 Hz, and iterative regression mode for the fit routine (unless otherwise stated). Note that it is important to split the averaging into more than one scan because the fitting routine provides the standard deviation between the different scan which can be used as error bars. However, these error bars should not be mistaken with the uncertainty of the actual measurement, which comprises more contributions, e.g., the uncertainty in the applied magnetic field. In virtually all data shown here, the visible scatter of the data does well-reflect these uncertainties returned by the fitting
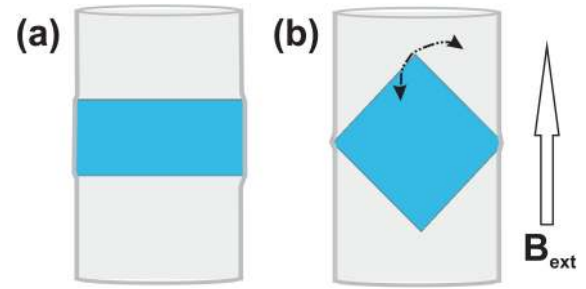


FIG. 2. Sketch of a low-background sample mounting inside a clear drinking straw. (a) Geometry if only in-plane magnetization curves are to be measured. (b) Square-shaped sample size which can be rotated from in-plane to out-of-plane geometry.

routine and therefore those error bars are not explicitly shown.

A clear drinking straw serves as sample holder where the sample is held in place by no other means than clamping it in-between the walls of the straw (see Fig. 2). If the magnetic field $B_{ext}$ shall only be applied in the plane of the film, a rectangular sample size of about $3 \times 5.5$ mm$^2$ is suitable [see Fig. 2(a)]; in cases where $B_{ext}$ shall be applied in- as well as out-of-plane, one should choose a square-shape sample with $4.2 \times 4.2$ mm$^2$ so that it can be rotated forth and back inside the straw [see Fig. 2(b)]. Finally, it shall be stressed again that with regard to the sample holder, great care has to be taken that the holder itself is homogeneous across the entire length of the gradiometer even while moving from the bottom- to the top-most position. Holes, cuts, and even small dents in the straw present locally missing diamagnetic material which the pickup system records as net-paramagnetic signal. In turn, textmarker labeling on the sample holder close to the sample behave oppositely, since textmakers are usually containing paramagnetic pigments. Similar care has to be exercised during handling of the samples to avoid any kind of magnetic contamination as pointed out before.[21–23] A good summary of inappropriate sample handling and mounting can be found in Ref. [22]. However, these precautions are not specific to SQUID magnetometry but also concerns other integral magnetic characterization techniques such as VSM or ferromagnetic or electron paramagnetic resonance techniques.

## B. Quantities and units relevant for magnetometry

The magnetization $M$ of a homogeneous sample of volume $V$ is related to the magnetic moment $m$ like $M = m/V$. Magnetometry is distinguished from susceptometry where the magnetic susceptibility tensor $\chi_{ij}$ is given by $\chi_{ij} = \partial M_i / \partial H_j$. Here $H$ denotes the magnetic field strength not to be mistaken with $B$ which is the magnetic flux density or magnetic induction. In the still rather common cgs units, $B$ is measured in Gauss (G), while $H$ is measured in Oersted (Oe), and in vacuum, both quantities are identical. In the proper SI units, $B$ is measured in Tesla (T) and $H$ is measured in A/m and, in vacuum, $B = \mu_0 H$; the conversion from cgs to SI is 10 000 G $= 1$ T. The MPMS uses by default the cgs-unit emu for $m$, which can be easily converted into the proper SI-unit

(1 emu $= 10^{-3}$ A m$^2$). Therefore, also the magnetization is often provided in emu/cm$^3$ in the literature which easily translates into the proper SI unit (1 emu/cm$^3$ = 1 kA/m). The externally applied magnetic field $H$ is provided in Oe by the magnetometer; since the corresponding SI unit A/m is rather uncommon, it is advisable to provide the external magnetic field in T and denote the quantity as $\mu_0 H$ to indicate that the value refers to the magnetic field strength outside the actual specimen where it is identical to $B$ and thus can be provided in the common SI unit Tesla.

In many publications, the measured quantity of SQUID magnetometry is often provided in emu/g which in the case of powder samples is easier to be measured and does not require an exact knowledge of the density of the used material. This has its benefits, e.g., in nanoparticulate samples where it is sometimes questionable if the density of the bulk material can be used. On the other hand, it makes the quantitative comparison between samples from different publications rather questionable. Even more intricate is to provide the results of magnetometry in $\mu_B$/atom. Here the number of atoms in the actual specimen has to be determined independently as atoms/cm$^3$. Then emu/cm$^3$ yields emu/atom which then is converted to $\mu_B$/atom using 1 $\mu_B = 9.274 \cdot 10^{-21}$ emu. The uncertainties of determining volume, density, or number of atoms in the sample may easily become larger than the actual uncertainty related to the magnetic measurement itself. In any case, it is advisable to either explicitly state the volume or mass of the measured sample separately or to provide the experimental result from magnetometry as measured, i.e., as $m$ in either emu or A m$^2$. This allows assessing the actual size of the measured signal and is of relevance for experiments close to the sensitivity limit of the magnetometer.

## C. Sensitivity and detection limits

SQUID magnetometers can be considered as one of the most sensitive types of quantitative magnetometry. Usually, the sensitivity of a SQUID device is of the order of fT/$\sqrt{\text{Hz}}$ which is far below the stray field of a single atomic layer of magnetic material of typical lateral dimensions in the range of few mm$^2$. In contrast, the sensitivity of commercial SQUID magnetometers is usually provided in emu; for the MPMS-XL5, it is $< 1 \cdot 10^{-8}$ emu below 250 mT and $< 2 \cdot 10^{-7}$ emu up to full field according to the manufacturers specifications. These specifications usually rely on a measurement with an empty sample holder (straw) and the typical value of artificial signal returned by the fitting routine. It, therefore, corresponds to the detection sensitivity of the entire pick-up coil detection system including fitting artifacts. Nevertheless, this sensitivity is a few orders of magnitude worse compared to the actual detection limit of a SQUID alone. On the other hand, $1 \cdot 10^{-7}$ emu roughly correspond to the magnetic moment of a single atomic layer of Ni, depending on the chosen specimen size. This translates to a fringing field of the order of nT in a distance of a few mm (see Ref. 9 and references therein). In Fig. 7, top right inset, a lastscan of a bare diamagnetic sapphire at 0 mT is shown where the fit routine returns a magnetic moment of $(3.6 \pm 0.8) \cdot 10^{-9}$ emu. So it is often the case that a single measurement can be recorded down to signals well below the specified sensitivity which in any case only provides an upper limit of a finite artifact signal upon measuring a true zero-signal.

For practical magnetometry, the specified sensitivity is, however, not the only relevant quantity to be considered. In many cases, in spintronics and magnetism, the actual magnetic specimen comes with a substrate or matrix which can be diamagnetic or paramagnetic. Due to the larger volume of the substrate compared to, e.g., a thin magnetic film already at moderate external magnetic fields, the diamagnetic moment of the substrate exceeds the ferromagnetic moment of the film because the diamagnetic moment increases linearly with field while the ferromagnetic moment quickly saturates with fields and stays constant. Therefore, to derive the magnetic properties of the specimen of interest, one has to subtract a large diamagnetic background from a large measured signal to derive the small magnetic moment of interest. This implies that the accuracy and reproducibility of a single measurement has to be sufficient to reliably derive the small magnetic signal of interest. In cases where the signal of interest is only 1% of the total measured signal, the accuracy and reproducibility of the measurement has to be better than $10^{-3}$ to obtain a magnetic signal with a sufficient signal to noise ratio of say 10. In other words, if SQUID measurements have to be corrected for the diamagnetic background of the specimen, it is not sufficient to detect signals of the order of $10^{-4}$ emu but one also has to assure an accuracy of $(1.000 \pm 0.001) \cdot 10^{-4}$ emu , i.e., an accuracy of the order of $10^{-7}$ emu. As it will be shown in this Tutorial, the commercial SQUID magnetometers are usually capable of delivering a sufficient accuracy of each individual measurement. In the case of the MPMS, this makes the use of the RSO option with a significant number of averaging necessary, since the standard or dc-transport offers insufficient scan speed to average over 50 individual movements for each measurement.

Finally, it has to be mentioned that for dia- (or para-) magnetic substrates, there is also a correlated uncertainty of the derived magnetic moment with the uncertainty of the externally applied magnetic field. As already mentioned, the field is never directly measured so that the nominal and the actual field experienced by the specimen are different. Consequently, if one calculates the diamagnetic contribution of the substrate from the nominal field, this results in small discrepancies to the actual diamagnetism due to the actual magnetic field experienced by the sample. This fact will be one of the main points of this Tutorial and severely limits the interpretation of as-recorded magnetic data from SQUID magnetometry in cases where substrates are used.

## III. DETAILS ON THE EXPERIMENTAL PROCEDURE

### A. Used specimen for magnetometry

Two types of magnetic specimen are exemplarily investigated here which are frequently found in current nanomagnetism and spintronic research. On the one hand, ultrasoft magnetic materials with a low coercive field ($H_c$) such as the $Ni_{80}Fe_{20}$ alloy, i.e., Permalloy (Py) are often used because of their low magnetic damping. On the other hand, dilute magnetic semiconductors (DMS) were intensively studied over

the past decade which usually have a rather low magnetic moment compared to the diamagnetic response of a typical substrate material it comes with. The following samples are under investigation: (i) A nominally 50 nm thick Py film grown on c-plane sapphire [Al$_2$O$_3$(0001)] by magnetron sputtering from a Py metal target using Ar at room temperature. X-ray diffraction confirmed that the film is virtually amorphous. FMR measurements on this sample revealed a rather narrow FMR line with a peak-to-peak width of 3 mT at a resonance field of 101.5 mT at 9.56 GHz which are typical values for good Py films. Therefore, a very narrow hysteresis with $H_c$ of about 0.1 mT can be expected for this Py film, see e.g., Ref. 25 and references therein. (ii) As typical DMS material, we rely on a previously well-studied DMS system, namely, $Zn_{0.8}Co_{0.2}O$ (Co:ZnO). One nominally 200 nm and one nominally 1 $\mu$m thick 20% Co:ZnO epitaxial films were grown on c-plane sapphire by reactive magnetron sputtering as described in detail elsewhere.[26] Detailed investigations using synchrotron radiation on the 200 nm[26] as well as the 1 $\mu$m[28] sample excluded the presence of metallic Co precipitations down to less than 1% relying on previously established quality indicators.[29] The 200 nm thick Co:ZnO film had been investigated by TEM and the two first layers adjacent to the sapphire substrate were found to be Co rich and Zn-deficient (see Fig. 6 of Ref. 27). The two typical magnetic specimen are complemented by (iii) a bulk Pd reference sample provided by Quantum Design and (iv) a bare c-plane sapphire substrate provided by CrysTec[30] from the same batch onto which the Py and Co:ZnO films have been grown.

## B. Standard measurement sequence

For almost any unknown type of magnetic specimen in the field of nanomagnetism and spintronics, a fully automated "standard sequence" is useful as a first test to specify the kind of magnetism of a given specimen. The standard sequence used throughout this work refers to the following experimental protocol: first, a full $M(H)$ curve is measured at 300 K from +5 T to −5 T and back using the "no overshoot" mode (field is approaching the desired magnetic field from one side and exactly stabilizes the magnetic field at the requested value; magnet is in persistent mode during the actual measurement). Then the sample is cooled down in +5 T to 2 K and another full $M(H)$ curve is recorded. Note that the $M(H)$ curve at 2 K is measured in field-cooled (FC) conditions which allows one to see whether exchange bias effects or field imprinted magnetizations of, e.g., uncompensated antiferromagnets[31] or ferrimagnets exist. If it is already known that they are present/absent, it may be advantageous to cool down in zero field between the 300 K and 2 K hysteresis. Subsequently, the field is lowered to 10 mT and an $M(T)$ curve is measured while warming the sample from 2 K to 300 K (field-heated, FH) using the sweep mode (no stabilization of the temperature for the actual measurement) with 0.5 K/min from 2 K to 20 K and with 5 K/min from 20 K to 300 K. Then, the field is set using no overshoot to −100 mT and to +50 mT and finally, to 0 mT using the "oscillation" mode (field overshoots the desired field and oscillates several

times around the target field with decreasing offset). The sample is then cooled down to 2 K in nominally zero-field. At 2 K the field is increased again to 10 mT and the identical $M(T)$ curve is measured under zero-field cooled (ZFC) conditions. Finally, another $M(T)$ curve is measured at 10 mT with identical step-sizes now cooling the sample from 300 K to 2 K (FC). It has to be noted that the actual field for the ZFC conditions is still finite and negative, i.e., antiparallel to the small probing field of 10 mT; if exactly zero field is required for ZFC, a magnet reset is needed (see further below). However, one should keep in mind that the manufacturer advises to avoid frequent resets to minimize the danger of damage to the magnet and, therefore, for an everyday standard sequence, a magnet reset is not a good option. Subsequently, additional and more detailed measurements can be taken, e.g., $M(H)$ curves under FC and ZFC conditions for exchange bias systems, $M(T)$ curves at remanence in cases where the sample is ferromagnetic/superparamagentic, and ZFC $M(T)$ curves with waiting times for spin glasses; here the actual magnetic properties of the given specimen decide, what protocol is appropriate.

Figure 3 shows the results of the standard sequence performed on the 200 nm thick 20% Co:ZnO film on sapphire. In Fig. 3(a), the as-recorded data for the $M(H)$ curves at 300 K and 2 K are shown. The maximum signal is of the order of 800 $\mu$emu. As can be seen from the negative slope it is dominated by a net-diamagnetic behavior which is superimposed by an additional contribution at 2 K. Since diamagnetism in this temperature range is a temperature independent quantity, one can easily derive the diamagnetic contribution from the slope of the $M(H)$-curve at 300 K at high magnetic fields. In this case, this yields $-1.8096(2) \cdot 10^{-8}$ emu/Oe, where the slope was taken in the range between 2 T and 5 T. This diamagnetic contribution of the sapphire substrate is then subtracted from all $M(H)$ and $M(T)$ data. The corrected $M(H)$ curves at 300 K and 2 K are shown in Fig. 3(b), which
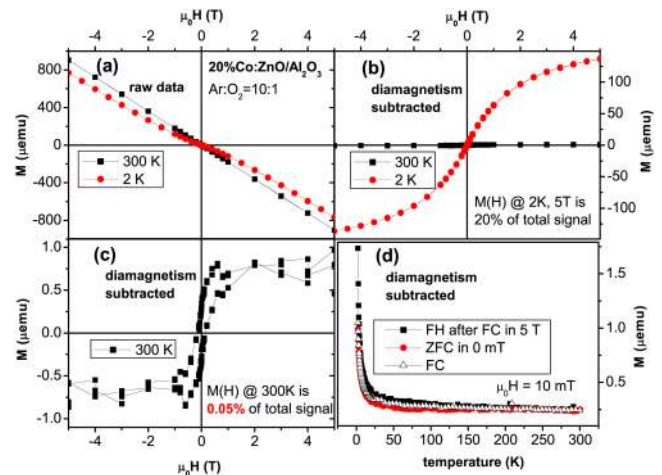
FIG. 3. Result of the standard sequence of a 200 nm thick 20% Co:ZnO film on sapphire. (a) displays the raw data of the $M(H)$ measurements at 300 K and 2 K, while in (b) the diamagnetic contribution of the substrate has been subtracted. (c) enlarges the $M(H)$ curve at 300 K where the total signal is of the order of the artifact level of the SQUID.[21] (d) summarizes the $M(T)$ measurements under field heated (FH), field cooled (FC), and zero field cooled (ZFC) conditions.

demonstrates that hardly any magnetic response beyond dia-magnetism is visible at 300 K. In contrast, a clear paramagnetic $M(H)$ curve is seen at 2 K, the size of which is only of the order of 120 $\mu$emu, i.e. roughly 20% of the total signal. In Fig. 3(c), the $M(H)$ curve at 300 K is enlarged which exhibits an apparent hysteresis; however, the overall size of the signal is only 0.05% of the total magnetic response of the specimen. Its absolute size is about 0.8 $\mu$emu and thus very close to the sensitivity limit which was reported before.[21] Consequently, the data are rather noisy and the visible scatter corresponds to the errorbars of each individual data point. In addition, it has clearly been demonstrated that this "hysteresis" stems from the residual pinned magnetic flux of the superconducting coil of the magnet and it inverts if a paramagnetic substrate is used rather than a diamagnetic one.[23] However, as we will show later-on for the 1 $\mu$m thick film, the response at 300 K contains an additional magnetic contribution beyond the artifact level stemming from the combination of the diamagnetic sapphire substrate and the residual field of the magnet.

Finally, Fig. 3(d) shows the three $M(T)$ curves which were subsequently measured under FH, ZFC, and FC conditions. At first sight, all three curves coincide rather well, all showing a $1/T$-like behavior which is typical for paramagnetic materials and consistent with the $M(H)$ curve in Fig. 3(b). However, a closer inspection reveals that while the FC and ZFC curve match rather well, the FH curve exhibits a slightly larger magnetization which is best seen at 2 K. Note that 20% Co:ZnO is right at the onset of the coalescence-induced magnetic order recently reported for Co:ZnO.[31] A similar behavior is also seen in the 1 $\mu$m thick film which will be discussed toward the end of this work.

## IV. EXPERIMENTAL DEMONSTRATION OF ARTIFACTS IN SQUID MAGNETOMETRY

This section is divided into three subparts: First, the Py film is investigated at 300 K applying the magnetic field in both principal orientations to extract $H_c$ as well as the anisotropy field $B_{aniso}$. The proper $H_c$ is only found if the residual field of the magnet is purged by resetting the magnet. Second, a simple procedure is introduced to quantify the offset field of the superconducting magnet depending on the setting mode. This is done for sapphire, the Pd reference as well as the Co:ZnO film. Finally, the 1 $\mu$m thick Co:ZnO sample is used to test the reproducibility of the standard sequence together with the variation of the offset field. This ultimately enables one to subtract the experimental data recorded for the sapphire substrate from the ones of the Co:ZnO film to derive the magnetic signal which stems from the interfacial magnetism in Co:ZnO.

### A. In-plane vs. out-of-plane hystereses for Py

Figure 4 shows an $M(H)$ curve of the Py/sapphire film recorded from +5 T to −5 T and back at 300 K. The magnetic field has been applied in the film plane (black circles) as well as out-of-plane (blue squares) by rotating the identical sample piece inside the straw [see Fig. 2(b)]. The high-field behavior of the $M(H)$ curves can be extrapolated to

determine the anisotropy field $B_{aniso}$ indicated by the orange star. Note that $B_{aniso}$ is actually a magnetic flux density but it is common to refer to it as "anisotropy field" and still provide values in Tesla. This procedure leads to $B_{aniso} = (1.0 \pm 0.1)$ T. Taking the area of the Py film and the film thickness of $(43 \pm 1)$ nm as derived by X-ray reflectivity (Fig. 4, inset), one can calculate the saturation magnetization $M_{sat}$ of this film yielding $(710 \pm 40)$ emu/cm$^3$ which would relate to $B_{aniso} = (0.9 \pm 0.5)$ T for an ideal thin film, i.e., $B_{aniso} = 4\pi M$. Considering that the Py film is grown on an oxide substrate and is unprotected against oxidation, one has to assume a by 10% reduced effective thickness, i.e., 2 nm of oxidized Py on either interface so that we consider the quantitative result in Fig. 4 as realistic. However, it is not the aim of this work to extract highly accurate quantitative numbers for $M$ and $B_{aniso}$ but to demonstrate the limitations of measuring a proper $H_c$ for Py with a SQUID magnetometer.

Figure 5(a) shows the low-field behavior of the data of Fig. 4. A clear hysteresis with an apparent $H_c$ of $(1.5 \pm 0.1)$ mT is visible in the in-plane data as well as a full remanence $M_R$. In contrast, a small residual hysteresis is also visible in the out-of-plane data although the hard axis $M(H)$ curve should be anhysteretic. However, considering that the sample is rotated inside the straw by two wooden sticks and only aligned by eye, one can assume that the orientation may not be truly out-of-plane. Taking $\sin^{-1}(M_R^{oop}/M_R^{ip}) = 1.8°$, one easily recognizes that the cause for the residual hysteresis out-of-plane is most likely due to an imperfect alignment. It is noteworthy that a mechanical sample rotator for the SQUID would have a background signal of the order of $10^{-4}$ emu, i.e., of the same order as the signal of the Py film itself.

More importantly, a close inspection of the in-plane data shows that actually no hysteresis but an *inverted* hysteresis is recorded as indicated by the arrows in Fig. 5(b). This totally unphysical behavior is due to the fact that a full $M(H)$ curve up to 5 T has been recorded to extract $B_{aniso}$, i.e., the magnet is in a state for which it exhibits a residual offset field. For example, coming from high positive fields toward zero field,
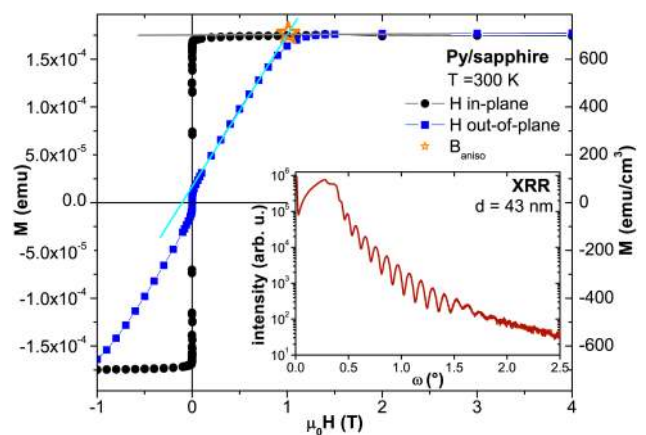


FIG. 4. In-plane (black circles) versus out-of-plane (blue squares) $M(H)$-curves for a $43 \pm 1$ nm thick permalloy (Py) film grown on sapphire to extract the anisotropy field $B_{aniso}$. The inset shows X-ray reflectivity to extract the actual film thickness to derive the magnetization (right scale).
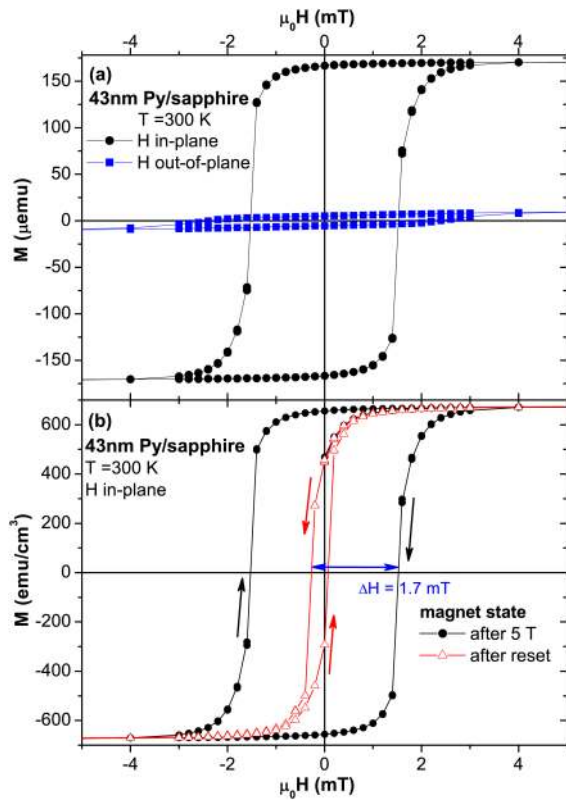
FIG. 5. (a) Enlargement of the low-field data of the measurement of Fig. 4 revealing an apparent coercive field for Py of 1.7 mT and a residual out-of-plane hysteresis. (b) Inverted in-plane hysteresis after the magnet has been at high magnetic fields (full circles) and a more realistic hysteresis after a magnet reset (open triangles).

the magnet is nominally still at small positive fields while the pinned flux already creates a negative residual field. This residual field is larger than the nominal field so that the magnetization switches before nominally zero field is reached. To prove that this is indeed the case one can use the so-called "magnet reset" option of the MPMS (see also Ref. 23). In the present case, the magnet is reset at a field of 10 mT and subsequently, an $M(H)$ curve is recorded only from $+10$ mT to $-10$ mT and back yielding the open triangles in Fig. 5(b). Now, an extremely narrow hysteresis with $H_c$ of less than 0.2 mT is visible which is much more realistic for Py (see Ref. 25). The hysteresis is not inverted any more (as indicated by the arrows) but a small shift of about 0.1 mT to the left is visible which should not be mistaken with an exchange bias effect. This small shift can also be attributed to an offset field which is still present after magnet reset; according to the manufacturer, the purification upon resetting the magnet is 0.1 to 0.2 mT so that such a small shift would be within specifications. It is noteworthy that this apparent horizontal shift of about 0.1 mT does not increase even after the magnet has been at 5 T as can be seen from the fact that both hystereses in Fig. 5(b) are shifted by the same amount. However, by comparing the two hystereses, one can estimate the offset field $\Delta H$ to be about 1.7 mT in this case, i.e., after the magnet has been at its full field of 5 T. It is, therefore, of utmost importance to reset the magnet and avoid larger magnetic fields well above 10 mT when a low $H_c$ of ultrasoft

magnetic materials such as Py shall be determined and the measurement sequence has to be adopted accordingly. Note that also in the case of ZFC conditions, a magnet reset may turn out to be unavoidable, e.g., in spin glass systems or if a complex sample system is cooled through its Néel temperature. If the magnet has been reset, and large fields are avoided, the offset field remains small and by that one can keep the number of resets as small as possible, e.g., by measuring low field $M(H)$ curves in a row. For the SQUID machine discussed here, maximum fields of 30 mT are possible without significantly increasing the residual field (not shown); however, the highest possible field to avoid an increase of the offset field may vary from magnet to magnet and has to be determined for each machine separately.

Finally, the $M(H)$ curve recorded in the out-of-plane geometry shall be inspected more closely. It has already been pointed out, based on simulations in Ref. 23, that in cases where $M$ and $H$ are not collinear, artifacts of the fitting routine of the MPMS come into play. Figure 6 shows again the $M(H)$ curves in the out-of-plane geometry of the Py film. At each field point, two measurements were taken, one with the iterative regression mode and one with the linear regression mode. The two side panels display the two raw scans, i.e., the SQUID voltage ($V_{\text{SQUID}}$) as a function of the sample
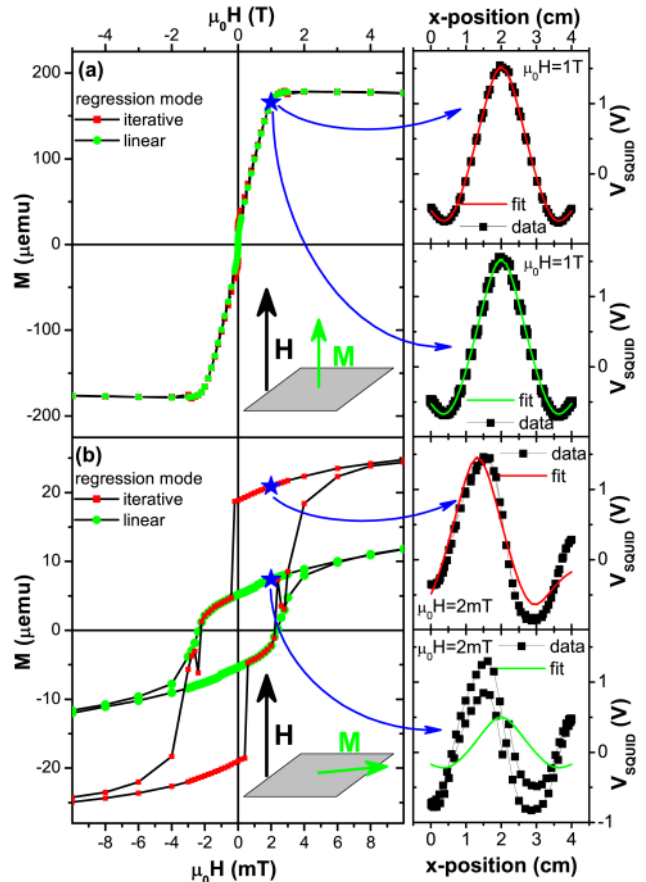


FIG. 6. (a) Out-of-plane hysteresis of Py measured with iterative (red squares) and linear (green circles) regression mode at 1 T. The corresponding raw scans (SQUID voltage versus sample position) indicate the respective data and the fit (see text). (b) Low-field behavior of the two measurements from (a) with the respective raw scans.

position (x position) along the pick-up gradiometer of the SQUID at 1 T, where $M$ is fully rotated out of the film plane by $H$. In the iterative regression mode (top), the expected stray field distribution of a point dipole is fitted to the measured raw data by allowing the sample's position to freely vary along x; $M$ is extracted from the amplitude of the fit. In linear regression mode, the position of the sample is fixed to the center of the x-position scan, in this case 2 cm. It is obvious from Fig. 6(a) that both fitting modes reproduce the raw data rather well and result in the identical value of $M$. If the field is lowered to 2 mT, $M$ is almost fully rotated back into the film plane since $H$ is not sufficient to overcome $B_{aniso}$. As Fig. 6(b) demonstrates, this leads to a strong discrepancy between the two fitting modes because the actual raw data resemble an "N" shaped distribution similar to what has been calculated for the non-collinear case before.[23] The iterative regression mode tries to follow one of the extrema to determine the apparently shifted sample position eventually jumping to the other which leads to rather discontinuous jumps in the $M(H)$ loop visible in Fig. 6(b) in the red squares with rather large values of $M$. In contrast, the linear regression mode results in a more realistic shape of the hysteresis although the quality of the fit appears to be worse [see side panels in Fig. 6(b)]. This phenomenon has theoretically been discussed in detail in Ref. 23 and there is no possibility to get an improved fit by the standard software of the magnetometer. Here it is important to remark that in cases where $M$ and $H$ can be non-collinear, e.g., in hard-axis magnetization curves, one has to either perform a tedious analysis with assumed exact position of the specimen and the angle of the magnetization with respect to the field by going into the raw data of the SQUID. Alternatively, one has to choose the linear regression mode to avoid erroneous results with regard to the shape of the $M(H)$ curve on the expenses of numerically incorrect values for $M$.

Once care is taken to avoid potential pitfalls in SQUID magnetometry, the magnetic properties of Py can be determined, although it possesses very low coercivity. A realistic order of magnitude of $H_c$ of 0.1 mT is derived which is not a trivial task for a 5 T superconducting magnet since $H_c$ is of the same size as the minimum residual field. Also the derived quantitative values for $B_{aniso}$ and $M_{sat}$ are within expectation for Py. Of course, an accurate determination of $H_c$ down to 0.01 mT for Py should rely on magnets with direct measurement of the applied field.

### B. Determination of the offset field

It has already been shown in Sec. IV A that the inverted hysteresis of the Py film suggests an offset field of about 1.7 mT at fields below 30 mT after the magnet has been at maximum field. Figure 7 shows a rather simple procedure to quantify it depending on the setting mode of the magnetic field. A bare sapphire substrate is used and first a standard sequence as described in the experimental details is recorded. The usual procedure to derive the diamagnetic signal of the sample is to take the slope of the high field behavior of the $M(H)$ curve at 300 K. A linear fit to the high field data leads to a diamagnetic susceptibility of

$(-1.117 \pm 0.001) \cdot 10^{-7}$ emu/mT for the used sapphire substrate. Since this procedure relies on high-field data above 2 T, small offset fields of the order of 2 mT do not significantly contribute to the uncertainty of the derived value for the susceptibility. After the standard sequence, the magnet has been at 5 T and is now set to nominally 0 mT (open stars) using the no-overshoot mode. Then, a single measurement is performed at nominally zero field which should result in zero magnetization for an ideal diamagnet. Figure 7, however, demonstrates that a small positive magnetization of $1.27 \cdot 10^{-7}$ emu is measured (top left raw data scan and full squares). Assuming that the sample indeed has zero magnetization, one can back-calculate this to a small negative residual field of 1.14 mT (full circles). Setting the field back to 10 mT in no-overshoot mode, a clear negative $M$ of $9.6 \cdot 10^{-7}$ emu is measured (bottom left raw scan), a value which exactly reproduces the results of the $M(T)$ measurements at 300 K during the standard sequence. Using the high field susceptibility, this translates into a real field of 8.6 mT corresponding to an antiparallel offset field of 1.4 mT. Going back to zero magnetic field, now using the oscillate mode, the initial result is reproduced. Also going back to 10 mT in
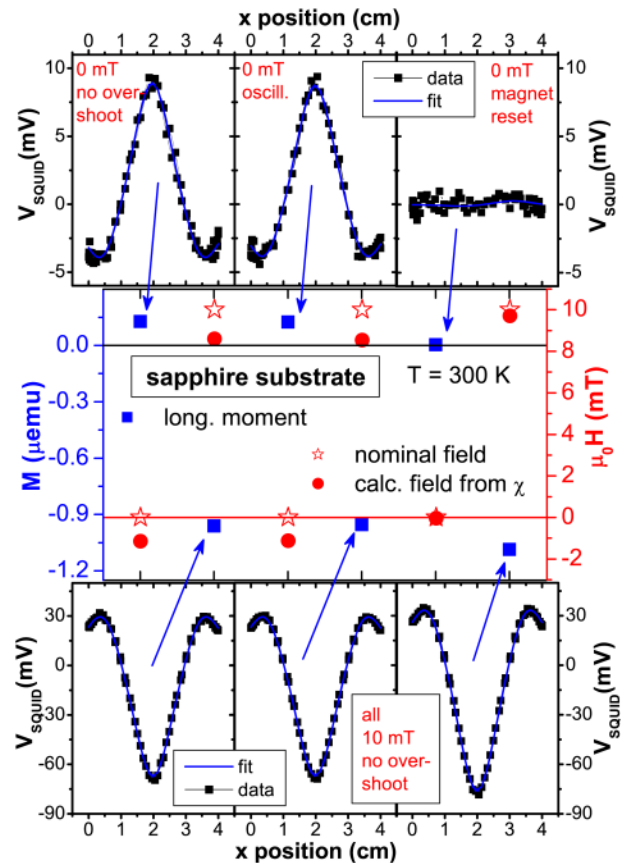


FIG. 7. Procedure to extract the offset field of the superconducting magnet depending on the setting mode of the field control for the case of a bare sapphire substrate. Full squares refer to the left axis and correspond to a series of subsequent individual SQUID measurements derived from the individual raw scans and corresponding fits which are shown in the respective insets. Each point corresponds to a different set mode and/or field value of the magnetic field which are denoted as follows: The open stars denote the nominal field value for the given measurement and full circles represent the back-calculated field values, both referring to the right axis, see text for details.

no-overshoot mode, the initial result is repeated. Obviously, the oscillatory mode starting from 10 mT is not sufficient to remove the trapped flux from the magnet. The magnet is then reset, i.e., heated to the normal conducting state from 10 mT so that the field is zero within 0.1 to 0.2 mT according to specifications. A virtually zero magnetization is measured (top right raw data in Fig. 7). The residual signal of $3.6 \cdot 10^{-9}$ emu is below the nominal detection sensitivity of the magnetometer and the back-calculated residual field is 0.03 mT, well below the specified accuracy. This small offset field is also consistent with the slight shift of the Py hysteresis of 0.1 mT after the magnet reset in Fig. 5(b). Going back to 10 mT, $1.08 \cdot 10^{-6}$ emu is measured which is in reasonable agreement with the susceptibility derived from the high-field data. We have chosen to show this behavior for 10 mT since this is a typical field used for recorded $M(T)$ curves throughout the literature, especially in the field of DMS. The reproducibility of this behavior has been tested also at slightly higher magnetic fields up to 30 mT and merely identical results have been found (not shown). Note that a magnet reset consumes the more liquid helium the higher the starting field is, therefore, it is also valuable to know that a magnet reset from only 10 mT is sufficient to reliably remove the residual field from trapped flux in the superconducting magnet.

Figure 8(a) displays the identical procedure for the paramagnetic Pd reference sample. Again a discrepancy of about 1.5 mT between the nominal field and the back-calculated one is found which only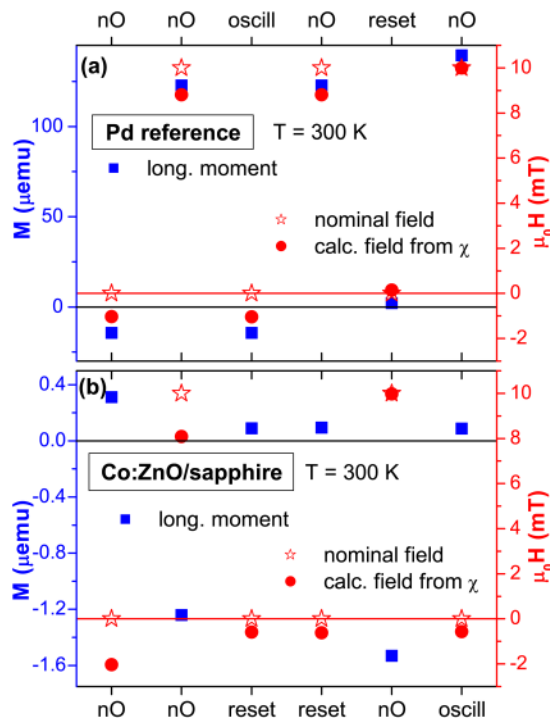 vanishes after the magnet has been reset. The fact that the residual magnetization is inverted by going from a diamagnetic to a paramagnetic material corroborates that the residual field is consistently antiparallel to the nominal field. In contrast, the $1\,\mu$m thick Co:ZnO sample depicted in Fig. 8(b) exhibits a significantly different behavior. Comparable to the bare sapphire substrate after the standard sequence, a small positive magnetization is measured at nominally 0 mT; however, back-calculating the actual field from the high-field diamagnetic response of that sample (in this case $-1.7 \cdot 10^{-7}$ emu/mT), the residual field is 2.0 mT, i.e., an actual field of 8 mT at nominally 10 mT. Also after resetting the magnet a small positive magnetization of $0.9 \cdot 10^{7}$ emu is measurable. This would correspond to a residual field of 0.6 mT which is, however, in disagreement with the previous findings where it was shown that a magnet reset leads to a residual field of only 0.1 mT which was consistently found for the Py hysteresis, the sapphire substrate and the Pd reference sample. A repeated reset does not change the result for Co:ZnO. Interestingly, the magnetization at 0 mT and 10 mT measured after the reset both significantly deviate compared to the ones before the reset. Obviously, the magnet reset has again removed the residual field so that the small remanent magnetization of the Co:ZnO sample cannot be taken as an artifact of the measurement. This will be discussed in more detail toward the end of Sec. IV C.

## C. Reproducibility of the standard sequence and trapped field for Co:ZnO

Having established that after a standard sequence, the magnet of the used MPMS has an antiparallel trapped field of 1.5 mT, this finding shall be verified and corrected by performing a series of subsequent standard sequences for the $1\,\mu$m thick 20% Co:ZnO sample. The motivation for the choice of the sample is as follows: (i) This piece of sample has been studied in great detail using x-ray diffraction, SQUID, and x-ray absorption spectroscopy over the past five years, see e.g., Refs. 26 and 28 and no indication of degradation over time has been found—other than for uncapped Py. (ii) This sample is paramagnetic so that at low temperature a finite magnetic response can be found—other than for sapphire where only a very small paramagnetic component exists which predominantly stems from Cr impurities as revealed by electron paramagnetic resonance (not shown). For sapphire, the $M(H)$ curves at 2 K and the $M(T)$ curves at low temperature are rather noisy since after subtraction of the predominant diamagnetic signal ($-5.5 \cdot 10^{-4}$ emu) only a very small paramagnetic signal of $2 \cdot 10^{-6}$ emu, i.e., 0.4% of the total signal is left over. This has been verified by two subsequent standard sequences (not shown). (iii) Figure 8 provides a first indication of a finite magnetic response of Co:ZnO at 300 K which was disregarded in previous publications[26] because of the well-known artifacts of the SQUID magnetometer.[21,23]

Figure 9(a) shows the $M(H)$ curves of four subsequent standard sequences at 2 K and the inset provides the 300 K data. Compared to the data in Fig. 3, the magnetic moment of this sample is much larger, which is due to the increased

FIG. 8. Identical procedure as in Fig. 7 for bulk Pd (a) and the $1\,\mu$m thick Co:ZnO film grown on sapphire (b); the measured magnetization is given by the full squares referring to the left axis, nominal (open stars) and back-calculated field (full circles) refer to the right axis. The setting mode of the field for each individual measurement is denoted by the horizontal axis labels; "nO" refers to no-overshoot mode.
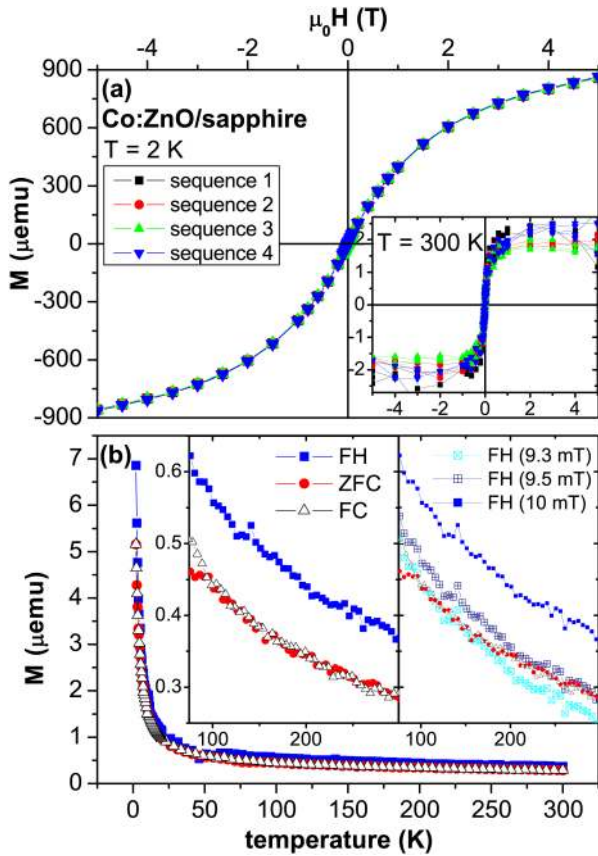
FIG. 9. (a) $M(H)$-curves for a Co:ZnO/sapphire film at 2 K and 300 K (inset). The identical sequence has been repeated four times. (b) $M(T)$ curves between 2 K and 300 K for FH (full squares), ZFC (full circles), and FC (open triangles) conditions. The insets enlarge the temperature region above 100 K revealing the different states of the magnet between FH and FC/ZFC conditions (see text).

layer thickness and the fact that a slightly larger piece has been measured. Again, the diamagnetic background has been derived from the slope of the high-field $M(H)$ data at 300 K and was already subtracted from all data in Fig. 9. The four sequences were performed as follows:

– The first standard sequence was directly measured after cooling down the magnetometer from room temperature without any waiting time to let the machine equilibrate thermally.
– The second one was directly measured after the first.
– For the third sequence, the temperature ramp for the $M(T)$ curves was at 0.5 K/min for the full temperature range. Consequently, the each $M(T)$ measurement took more than 3 h longer compared to the standard sequence, where the temperature above 20 K is ramped at 5 K/min.
– Finally, the fourth sequence has been measured after the sample had been removed from the magnetometer and the sample holder straw and was remounted after three days in a new straw.

It is obvious that the four $M(H)$ curves are highly reproducible at both temperatures, although at 300 K, some noise is clearly visible; the $M(T)$ curves are discussed further below in Fig. 10(c). This good reproducibility of the $M(H)$ curves is rather remarkable and the prerequisite to be able to

reliably subtract data recorded for two different specimens from each other.

Figure 9(b) displays the $M(T)$ measurements under FH, ZFC, and FC conditions of the first sequence, for better clarity, the error bars are omitted since they hardly exceed the visible scatter of the data. Except for a small discrepancy at very low temperatures between the FH and the two other curves, all three curves coincide well which is consistent with the findings for the 200 nm Co:ZnO film in Fig. 3(d). However, enlarging the $M(T)$ data between 100 K and 300 K, one can recognize that up to 300 K, the FH data deviate from the FC and ZFC ones by about $1 \cdot 10^{-7}$ emu (left inset). Slightly altering the actual magnetic field for correcting the diamagnetic background (right inset) reveals that the argument to assume a difference in actual magnetic field of $0.6 \pm 0.1$ mT makes the FH data coincide with the FC/ZFC ones at elevated temperatures. The argument to assume a small discrepancy between FH and the FC/ZFC measurements can be found in the procedure to set the magnetic field to 0 mT before the ZFC experiment. Other than in Figs. 7 and 8, the field is not oscillated to zero from 10 mT but from 50 mT which obviously alters the state of the residual field. This finding is in agreement with the fact that the procedure in Sec. II only leads to reproducible results up to 30 mT. Note that a magnet reset before ZFC makes the discrepancy between the FH and the FC/ZFC worse because then the overall offset field of 1.4 mT which is present in the FH $M(T)$ curve would be removed for the ZFC and FC $M(T)$ curves by the reset.

Figure 10 provides further insight into the behavior of the offset field. It has already been pointed out that the size of the offset field scales with the field strength.[23] So far, only its influence at low magnetic fields around 10 mT has been evidenced by the inverted Py hystereses and the $M(T)$ curves of Co:ZnO. Turning to the high field behavior of the offset field, one can remove the residual $M(H)$ hysteresis at 300 K by assuming a residual antiparallel offset field before the diamagnetic background is removed. For that one first determines the diamagnetic background as described before. The one subtracts a small offset field from the magnetic field data, e.g., 50 000 Oe → 49 990 Oe, 40 000 Oe → 39 990 Oe, etc. Then one uses these assumed field values to subtract the diamagnetic contribution as derived before. The resulting $M(H)$ curves then change and the apparent magnetization at high fields gets smaller or even negative. This has to be repeated for different assumed offset fields until the magnetization at high fields is zero. Figure 10(b) demonstrates that zero magnetic response from 1 T to 5 T can be derived if a constant offset field of 12.5 mT is assumed, which is still within specifications of 1% field accuracy of the MPMS. One has to remark that the 12.5 mT only represents an upper limit for the offset field for the given magnetometer in Linz; the MPMS in Warsaw behaves slightly different at high magnetic fields (see Figs. 6, 7, and 9 in Ref. 23); however, the order of magnitude is consistent with the findings reported there. It has to be noted that this procedure would eliminate eventual ferro- or superparamagnetic contributions in the 300 K $M(H)$ curves; we will come back to this point further below.

First, the reproducibility of the offset field at low fields shall be studied for this realistic DMS sample. For that
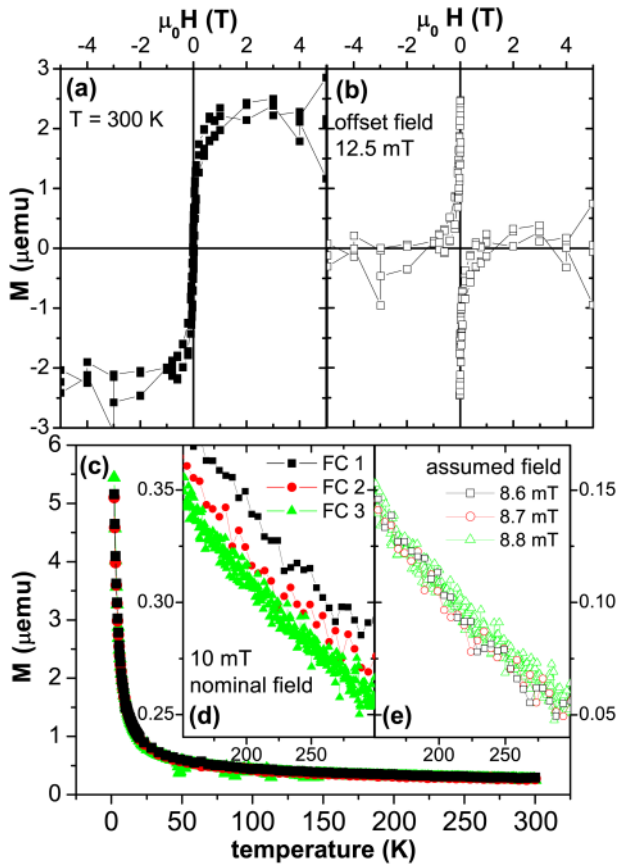
FIG. 10. (a) Residual apparent hysteresis of Co:ZnO/sapphire at 300 K. (b) Assumed offset field of 12.5 mT to bring the data to zero between 1 T and 5 T. (c) Three consecutive $M(T)$ curves of the sequences in Fig. 9 under FC conditions. (d) Enlargement of the behavior above 150 K assuming the nominal field. (e) $M(T)$ curves corrected by the offset field from Fig. 7.

Fig. 10(c) exemplarily compiles the FC $M(T)$ curves of the first three standard sequences of the Co:ZnO sample which fall on top of each other rather well. This result is of interest as well because in the third sequence, the entire measurement took more than 3 h longer than the other two FC curves. The good agreement between the three FC curves demonstrates that no time-dependent relaxations neither of the magnetic field nor the magnetic specimen itself occur. It also proves that the sample is always in thermal equilibrium even if a rather quick ramp of 5 K/min is used. Obviously, the previously reported temperature drifts in old MPMS machines in Ref. 17 are avoided in the present version of the magnetometer or the influence of the temperature drift on the magnetic properties is negligible. Figure 10(d) enlarges the three FC curves between 150 K and 300 K where the nominal field of 10 mT has been used to correct the diamagnetic background. Small discrepancies are visible which, however, can be removed by slightly varying the assumed offset field. Since we already know that the offset field has to be around 1.5 mT, the actual field has to be about 8.5 mT. Figure 10(e) shows that it is sufficient to vary the offset field by only 0.1 mT to yield coinciding FC curves over the entire temperature range between 150 K and 300 K within the noise level. Therefore, taking together all presented results, we can conclude that the offset field

of this magnet at low magnetic fields around 10 mT is $(1.6 \pm 0.1)$ mT after the magnet has been at the full field of 5 T. Note that we refrained from repeating all the above tests for the resulting offset field and its reproducibility for lower maximum fields between 1 and 4 T. In case a specific specimen shall be investigated, one can easily adopt the preceding procedure for lower (or higher, if one, e.g., has the MPMS XL7) maximum fields.

Turning back to the offset field above 1 T, we have repeated the procedure in Fig. 10(b) for the $M(H)$ curves at 300 K of the three full standard sequences of the Co:ZnO and the two of the bare sapphire (not shown). It turns out that for Co:ZnO, the assumed offset field to remove the residual $M(H)$ curve is $(11 \pm 1)$ mT, while for sapphire only $(6 \pm 1)$ mT are needed to yield zero magnetic response at high magnetic fields, i.e., pure diamagnetic behavior. Given the high reproducibility of the behavior of the offset fields in general, this again corroborates that for Co:ZnO an additional magnetic signal exists at 300 K. Since the residual $M(H)$ curves are highly reproducible [see inset of Fig. 9(a)], this implies that also the behavior of the offset field is reproducible and can be taken into account to correct measured data once it has been determined for a given magnet. In other words, if the upper limit of the true offset field is $6 \pm 1$ mT as seen for sapphire, it has to be the same for Co:ZnO on sapphire. However, since it is necessary to assume a larger offset field for Co:ZnO of $11 \pm 1$ mT, this indicates that one has also eliminated a true ferromagnetic contribution beyond the offset field in Fig. 10(b). Since the existence of a ferromagnetic contribution was already indicated before [see Fig. 8(b)], one can go ahead and try to separate the ferromagntic signal of the Co:ZnO from the sapphire.

In turn, the results for sapphire suggest that the offset field of the used magnetometer only ranges from $(1.6 \pm 0.1)$ mT at low fields below 10 mT to 6 mT at fields above 1 T together with a transition regime between 30 mT and 1 T which is, however, not investigated in more detail here. In principle, one could repeat the procedure as shown in Fig. 10(b) with an assumed offset field with varying size and write a fitting sequence to turn the sapphire signal to zero at all fields to get the full behavior of the true offset field. Note that this assumes in contrast to Ref. 20 that sapphire is purely diamagnetic. We think that this assumption is justified since we were never able to alter the residual magnetic signal for sapphire by cleaning, etching, or cleaving and also highly pure Si or GaAs were always exhibiting similar residual hystereses. On the other hand, the procedure described in the following will automatically remove the influence of the offset field.

Finally, having established the high reproducibility of the magnetometer from sequence to sequence as well as the presence of an additional magnetic signal in Co:ZnO at 300 K, this signal can be extracted from the data. Figure 11 shows the $M(H)$ curves for the bare sapphire and the Co:ZnO film. The diamagnetic susceptibility determined from the high-field $M(H)$ slope has been taken to scale the magnetic moment measured in the two data sets. The diamagnetic susceptibility is dominated by the sapphire (thickness of 0.5 mm in contrast to $1 \mu$m for the Co:ZnO film) so that the
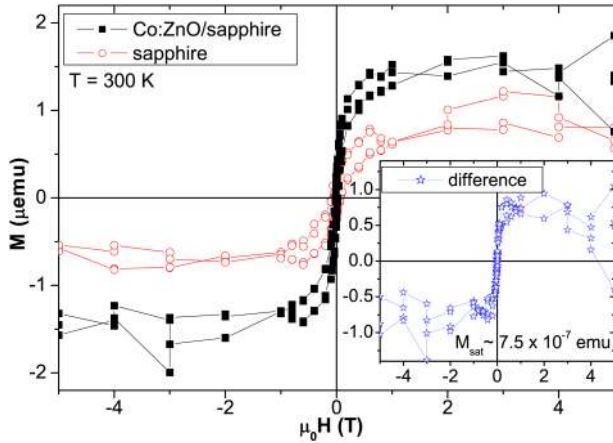
FIG. 11. Residual apparent hysteresis in the $M(H)$ curves of Co:ZnO/sapphire (full squares) and bare sapphire (open circles) at 300 K. The inset shows the direct difference of the two measurements revealing a residual saturation magnetization $M_{sat}$ for Co:ZnO of about $7.5 \cdot 10^{-7}$ emu.

susceptibility is a measure for the volume (in fact, area for a given substrate thickness) of the respective specimen. The inset of Fig. 11 shows the direct difference of the two measurements revealing a saturation moment of $7.5 \cdot 10^{-7}$ emu with a visible scatter, i.e., accuracy of $3 \cdot 10^{-7}$ emu so that the signal to noise ratio is only slightly larger than 2. Looking at the low field behavior, it turns out that within the noise level there is no significant hysteresis visible (not shown). It is, therefore, plausible to assume that this residual signal is superparamagnetic in nature, i.e., a Langevin-type anhysteretic $M(H)$ curve at 300 K as reported for Co:ZnO before.[29] Turning to the absolute size of the signal, metallic Co has a magnetic moment of $1.72 \mu_B$[9] while $Co^{2+}$ in ZnO has a moment of $3.4 \mu_B$,[31] the former being ferromagnetic, the latter paramagnetic, i.e., strongly temperature dependent. One Bohr magneton corresponds to $9.3 \cdot 10^{-21}$ emu so that about $5 \cdot 10^{13}$ metallic Co atoms contribute to the magnetic signal in Fig. 11. Note that assuming only $Co^{2+}$ as source of the magnetic signal, it would correspond to $2.5 \cdot 10^{13}$ $Co^{2+}$ ions. In contrast, the total number of Co atoms/ions in the sample is about $2 \cdot 10^{17}$, which can be calculated from the Co content of 20%, the volume of the Co:ZnO film as well as molar mass (81.38 g/mol) and density (5.606 g/cm$^3$) of ZnO. This estimate yields that a fraction of 0.03% of the total number of Co atoms in the sample are present as metallic Co and contribute to the signal in Fig. 11. In turn, $5 \cdot 10^{13}$ metallic Co atoms are of the order of a single atomic layer of Co. In that regard, the amount of Co in the Co-rich two interface layers evidenced by TEM[27] would already be sufficient to account for the size of the signal recorded by the SQUID at 300 K.

## V. SUMMARY

We have presented a range of measurements using a commercial MPMS-XL5 SQUID magnetometer to illustrate how to extend these measurements to higher ultimate performance. The history-dependent offset field of the superconducting magnet was characterized to be taken into account for obtaining more realistic results for samples with low coercive fields $H_c$ or very low magnetic moments.

For Py, i.e., low coercive fields, one is in the regime where the magnet needs to be reset and magnetic fields higher than 10-30 mT shall be avoided. This assures that the offset field remains below 0.1 mT and one can derive realistic $H_c$ values for Py. In contrast, in cases where the magnet had been at its maximum field of 5 T, the offset field is at least $1.6 \pm 0.1$ mT even at fields below 30 mT. Since, in all cases, the offset field is antiparallel to the preceding high magnetic field, this leads to an inverted hysteresis and misleading apparent coercive fields [see Fig. 5(b)].

In cases where $M(H)$ curves shall be traced over the entire field range, the offset field cannot be avoided and separate low- and high-field hystereses should be traced as for Fig. 5. In the course of a full $M(H)$ cycle, the offset field ranges from 1.6 mT at low fields below 30 mT up to 6 mT at high fields from 1 T to 5 T giving rise to residual $M(H)$ curves for diamagnetic substrates [see Figs. 10(a) and 11] which are inverted for paramagnetic substrates (see Ref. 23). Such residual hystereses stemming from the offset field of the superconducting magnet limit the useful sensitivity of the SQUID magnetometer (see Ref. 21). Finally, in cases of non-collinear situations between $M$ and $H$, like in hard-axes $M(H)$ curves, the proper fitting mode has to be taken into account (see Fig. 6).

It should be stressed again that the actual offset field and its field dependence is determined by the actual magnet so that the quantitative results presented here can be different for other machines; this is particularly true for the high field behavior (see Ref. 23), where the high field offset field of the Warsaw SQUID is found to be not linear with the previously applied maximum field. The individual behavior of each magnet depends on its history since the residual flux is often pinned at defects and events in the past such as frequent quenches of the magnet (but also too frequent magnet resets) may influence the behavior and also lead to changes with time for a given magnet. It is, therefore, important to have easy-to-handle tests like the ones presented here to determine the actual behavior of the magnet from time to time if measurements at the performance limit are to be carried out.

Once the offset field for a given magnetometer is characterized, e.g., by a simple procedure as in Figs. 7 and 8, it can be taken into account to correct the measured data. In the present case, the measurements on the Py film in Fig. 5 corroborate the size of the offset field independently. We have demonstrated that the magnetometer offers a very high reproducibility of the results (see Fig. 9) and time dependent effects can be ruled out to some extent. In particular, deviating $M(T)$ curves do not originate from a time dependent relaxation of the (pinned) flux in the superconducting magnet on time-scales up to several hours [see Fig. 10(c)]. The good reproducibility explicitly includes the size of the offset field after large magnetic fields which was found to be reproducible within 0.1 mT even if two $M(H)$ and three $M(T)$ curves of a standard sequence have been measured in-between [see Fig. 10(e)].

Having established all the above, one is well-prepared to disentangle very small magnetic signals such as the ones shown in Fig. 11 for 20% Co:ZnO from both the predominating diamagnetism from the sapphire substrate as well as from most of the measurement artifacts stemming from the pinned

residual flux in the superconducting magnet. This allows one to extract from integral magnetometry magnetic signals corresponding to about $5 \cdot 10^{13}$ metallic Co atoms. In the present case, this signal is attributed to two Co-rich and Zn-deficient atomic layers right at the interface between Co:ZnO film and sapphire substrate which was evidenced by tedious TEM investigations in Ref. 27. Despite all efforts to correct for the known artifacts of integral SQUID magnetometry, the resulting signal is, however, rather noisy and not much can be said about the actual magnetic properties, which are presumably superparamagnetic; nevertheless, the experiment in Fig. 8(b) suggests a finite remanence of less than $1 \cdot 10^{-7}$ emu for Co:ZnO so also soft ferromagnetic behavior of these interfacial layers is possible as well. Although no definite conclusions can be drawn from the integral SQUID measurement alone, the work presented here may still be useful for other SQUID users to avoid several pitfalls in such types of magnetometry. On the other hand, it is remarkable that one can trace down the magnetic signal of only two atomic layers of a $1 \mu m$ thick film which are otherwise only traceable with very detailed and tedious TEM work. Vice versa, it demonstrates the very high sensitivity of SQUID magnetometry, which, however, requires careful correction of several possible artifacts. While the actual origin of such small magnetic signals can only be given by careful additional characterization like in Ref. 27, the relative ease and ultimate sensitivity of magnetic characterization relying on SQUID magnetometry already gives the first evidence that more in-depth characterization is required.

Finally, the reader shall be aware that the focus of this Tutorial is rather narrow. The main emphasis is put on artifacts related to trapped flux in the superconducting magnet from the perspective of people working in the field of nanomagnetism and spintronics, i.e., the SQUID is challenged by low moment samples (on large diamagnetic backgrounds) or low coercive fields. Other potential pitfalls have been already discussed elsewhere in sufficient detail, e.g., the issues related to the fitting routine in Refs. 16, 18, 19, and 23 or improper sample handling and mounting in Refs. 21 and 22. Also for the underlying physics of SQUIDs, the reader shall be again referred to a comprehensive review.[8]

*Note added in proof.* Very recently a very instructive article about how to increase the sensitivity of SQUID magnetometery by intruducing a compensating sample holder has been put onto the arXiv:1809.02346.

## ACKNOWLEDGMENTS

[1] S. Foner, J. Appl. Phys. **79**, 4740 (1996).
[2] Z. Q. Qiu and S. D. Bader, Rev. Sci. Instrum. **71**, 1243 (2000).
[3] G. P. Felcher, J. Appl. Phys. **87**, 5431 (2000).
[4] H. A. Dürr, T. Eimüller, H.-J. Elmers, S. Eisebitt, M. Farle, W. Kuch, F. Matthes, M. Mertins, H.-C. Mertins, P. M. Oppeneer, L. Plucinski, C. M. Schneider, H. Wende, W. Wurth, and H. Zabel, IEEE Trans. Magn. **45**, 15 (2009).
[5] C. S. Arnold, M. Dunlavy, and D. Venus, Rev. Sci. Instrum. **68**, 4212 (1997).
[6] C. P. Poole, *Electron Spin Resonance: A Comprehensive Treatise and Experimental Techniques* (Dover Publications Inc., 1997).
[7] M. Farle, Rep. Prog. Phys. **61**, 755 (1998).
[8] R. L. Fagaly, Rev. Sci. Instrum. **77**, 101101 (2006).
[9] A. Ney, P. Poulopoulos, and K. Baberschke, Europhys. Lett. **54**, 820 (2001).
[10] N. Fontaina-Troitino, S. Liebana-Vinas, B. Rodriguez-Gonzalez, Z.-A. Li, M. Spasova, M. Farle, and V. Salgueirino, Nano Lett. **14**, 640 (2014).
[11] M. Sawicki, T. Devillers, S. Galeski, C. Simserides, S. Dobkowska, B. Faina, A. Grois, A. Navarro-Quezada, K. N. Trohidou, J. A. Majewski, T. Dietl, and A. Bonanni, Phys. Rev. B **85**, 205204 (2012).
[12] J. Sanchez-Barriga, A. Varykhalov, G. Springholz, H. Steiner, R. Kirchschlager, G. Bauer, O. Caha, E. Schierle, E. Weschke, A. A. Ünal, S. Valencia, M. Dunst, J. Braun, H. Ebert, J. Minar, E. Golias, L. V. Yashina, A. Ney, V. Holy, and O. Rader, Nat. Comm. **7**, 10559 (2016).
[13] J.-P. Cleuziou, W. Wernsdorfer, V. Bouchiat, T. Ondarcuhu, and M. Monthioux, Nat. Nanotechnol. **1**, 53 (2006).
[14] Quantum Design, Inc., 10307 Pacific Center Court, San Diego, CA 92121, USA, see www.qdusa.com.
[15] Cryogenic Ltd, Unit 6, Acton Park Industrial Estate, The Vale, London W3 7QE, UK, see www.cryogenic.co.uk.
[16] A. Zieba, Rev. Sci. Instrum. **64**, 3357 (1993).
[17] Y. Kopelevich and S. Moehlecke, Physica C **253**, 325 (1995).
[18] L. L. Miller, Rev. Sci. Instrum. **67**, 3201 (1996).
[19] P. Stamenov and J. M. D. Coey, Rev. Sci. Instrum. **77**, 015106 (2006).
[20] R. Salzer, D. Spemann, P. Esquinazi, R. Höhne, A. Setzer, K. Schindler, H. Schmidt, and T. Butz, J. Magn. Magn. Mater. **317**, 53 (2007).
[21] A. Ney, T. Kammermeier, V. Ney, K. Ollefs, and S. Ye, J. Magn. Magn. Mater. **320**, 3341 (2008).
[22] M. A. Garcia, E. Fernandez Pinel, J. de la Venta, A. Quesada, V. Bouzas, J. F. Fernandez, J. J. Romero, M. S. Martin Gonzalez, and J. L. Costa-Krämer, J. Appl. Phys. **105**, 013925 (2009).
[23] M. Sawicki, W. Stefanowicz, and A. Ney, Semicond. Sci. Technol. **26**, 064006 (2011).
[24] Quantum Design 2001 MPMS Application Note 1014-208 A: Remnant fields in MPMS superconducting magnets.
[25] L. F. Yin, D. H. Wei, N. Lei, L. H. Zhou, C. S. Tian, G. S. Dong, X. F. Jin, L. P. Guo, Q. J. Jia, and R. Q. Wu, Phys. Rev. Lett. **97**, 067203 (2006).
[26] A. Ney, V. Ney, M. Kieschnick, K. Ollefs, F. Wilhelm, and A. Rogalev, J. Appl. Phys. **115**, 172603 (2014).
[27] A. Kovacs, A. Ney, M. Duchamp, V. Ney, C. B. Boothroyd, P. L. Galindo, T. C. Kaspar, S. A. Chambers, and R. E. Dunin-Borkowski, J. Appl. Phys. **114**, 172603 (2013).
[28] V. Ney, F. Wilhelm, K. Ollefs, A. Rogalev, and A. Ney, Phys. Rev. B **93**, 035136 (2016).
[29] A. Ney, M. Opel, T. C. Kaspar, V. Ney, S. Ye, K. Ollefs, T. Kammermeier, S. Bauer, K.-W. Nielsen, S. T. B. Goennenwein, M. H. Engelhard, S. Zhou, K. Potzger, J. Simon, W. Mader, S. M. Heald, J. C. Cezar, F. Wilhelm, A. Rogalev, R. Gross, and S. A. Chambers, New J. Phys. **12**, 013020 (2010).
[30] CrysTec GmbH, Köpenicker Str. 325, 12555 Berlin, Germany, see www.crystec.de.
[31] V. Ney, B. Henne, J. Lumetzberger, F. Wilhelm, K. Ollefs, A. Rogalev, A. Kovacs, M. Kieschnick, and A. Ney, Phys. Rev. B **94**, 224405 (2016).